Statistical distribution of binary ligands within rhodium–organic octahedra tunes microporosity in their assemblies

Tomoki Tateishi,[a] Javier Troyano,[a,b,c] Shun Tokuda,[a,d] Gavin A. Craig,[a,e] Simon Krause,[f] Alfredo López-Olvera,[g] Ilich A. Ibarra[g] and Shuhei Furukawa[a,d,*]

Structure–porosity relationships for metal–organic polyhedra (MOPs) are hardly investigated because of the difficulty in structural characterization. Here, we show a mixed ligand strategy to statistically distribute two distinct carbazole-type ligands within rhodium-based octahedral MOPs, leading to systematical tuning of the microporosity in the resulting amorphous solids.

Metal–organic polyhedra (MOPs) are a class of molecules with an intrinsic void and are synthesized by connecting designed organic links with metal nodes.[1,2] MOPs can be further assembled to fabricate new porous solids with a variety of material shapes, including crystals,[3] gels,[4] films[5] and mixed-matrix membranes.[6] In these materials, the key to achieving permanent porosity is to exploit the extrinsic porosity between MOPs, in addition to the intrinsic voids of MOPs.[7]

Crystalline MOP systems are more commonly investigated than their amorphous systems[8] because they allow for the exact structure determination by single-crystal X-ray diffraction experiments in a similar way to metal-organic frameworks (MOFs).[9] However, unlike MOFs, MOPs are packed by weak interactions and it is hard to elucidate the structure–porosity relationship for the MOP systems. This is because the packing arrangement of MOPs can change after the removal of solvent molecules — also known as activation — that is indispensable for the evaluation of porosity prior to the sorption experiments. This change in packing alters extrinsic pores between MOPs and often leads to the loss of the long-range order, thus the amorphization.[10,11]

Another issue for the evaluation of porosity in MOPs relies on the stability of MOPs against the activation process.[12] Some MOPs decompose after the activation; however, it is hard to distinguish between the MOP decomposition and the amorphization from the powder X-ray diffraction (PXRD) experiments. The structural integrity of MOPs requires further spectroscopic/spectrometric characterization to evaluate the porosity inside MOPs accurately. An approach to tackle this issue is to use Rh-based MOPs that are known to be thermally stable for the general activation process.[13]

To date, some researchers tried to systematically evaluate a structure–porosity relationship using prototypical cuboctahedral MOPs [$M_{24}(bdc)_{24}$] with isophthalate derivatives (bdc) of which different functional groups on the 5-position. The functional groups on the MOP surface change the packing arrangement of MOPs.[14] A MOP with suitably bulky groups showed one of the highest porosity,[15] while in many cases the functionalization led to a decrease in porosity compared to the non-functionalized MOP.[16] These results indicate that the high porosity stems from loose packing of MOPs, and the decreased porosity is most likely due to pore blocking by functional groups. The balance between the loose packing and the pore blocking should be determined by the interaction between MOPs. To tune such intermolecular interaction, one approach is to generate the complexity on the surface of MOPs. Indeed, there are few studies to induce such complexity by physically mixing multiple homoleptic cages[17] or molecularly mixing multiple ligands to form heteroleptic cages;[18–20] however, the structure-porosity relationship of MOPs with such chemical complexity is still unclear.

Here we show another approach to tuning the microporosity in the amorphous solids of MOPs by systematically changing the composition of two mixed ligands in a series of MOPs. We chose an octahedral-type MOP[21–23] because of its simpler geometry and fewer numbers of components than the prototypical cuboctahedral MOP.[17,19] We newly synthesized two octahedral Rh(II)-based MOPs with 9*H*-carbazole dicarboxylate

[a] *Institute for Integrated Cell-Material Sciences (WPI-iCeMS), Kyoto University, Yoshida, Sakyo-ku, Kyoto 606-8501, Japan. E-mail: shuhei.furukawa@icems.kyoto-u.ac.jp*
[b] *Department of Inorganic Chemistry, Autonomous University of Madrid, 28049 Madrid, Spain.*
[c] *Institute for Advanced Research in Chemical Sciences (IAdChem), Autonomous University of Madrid, 28049 Madrid, Spain.*
[d] *Department of Synthetic Chemistry and Biological Chemistry, Graduate School of Engineering, Kyoto University, Katsura, Nishikyo-ku, Kyoto 615-8510, Japan.*
[e] *Department of Pure and Applied Chemistry, University of Strathclyde, Glasgow, G1 1XL, UK.*
[f] *Nanochemistry department, Max Planck Institute for Solid State Research, 70569 Stuttgart, Germany.*
[g] *Laboratorio de Fisicoquímica y Reactividad de Superficies (LaFReS), Instituto de Investigaciones en Materiales, Universidad Nacional Autónoma de México, Circuito Exterior s/n, CU, Del Coyoacán, 04510 México D.F., Mexico.*

† Electronic Supplementary Information (ESI) available: Details of synthetic procedures, crystallographic data, IR, NMR, MALDI-TOF mass, UV-Vis spectra, PXRD data, TGA data, gas sorption data and cif files for **HCzRhMOP** and **BnCzRhMOP**. CCDC 2325101 and 2325135. For ESI and crystallographic data in cif or other electronic format see DOI:

derivatives: [$Rh_{12}(HCz)_{12}$] (**HCzRhMOP**) and [$Rh_{12}(BnCz)_{12}$] (**BnCzRhMOP**), HCz = 9*H*-carbazole-3,6-dicarboxylate[22,24] and BnCz = 9-benzyl-9*H*-carbazole-3,6-dicarboxylate.[23] To tune the interaction between the MOPs, we further synthesized mixed-ligand **H/BnCzRhMOPs** of [$Rh_{12}(HCz)_{12-x}(BnCz)_x$] in various ratios of HCz and BnCz (x = 1, 3, 6, 9 and 11 for HCz/BnCz = 11/1, 9/3, 6/6, 3/9 and 1/11, respectively). **HCzRhMOP**, **H/BnCzRhMOPs** and **BnCzRhMOP** showed the linear correlation of their porosity with the number of the benzyl groups. These results indicate that the systematic variation of MOP compositions highly influences the packing arrangement of MOPs and the resulting microporosities (Fig. 1).

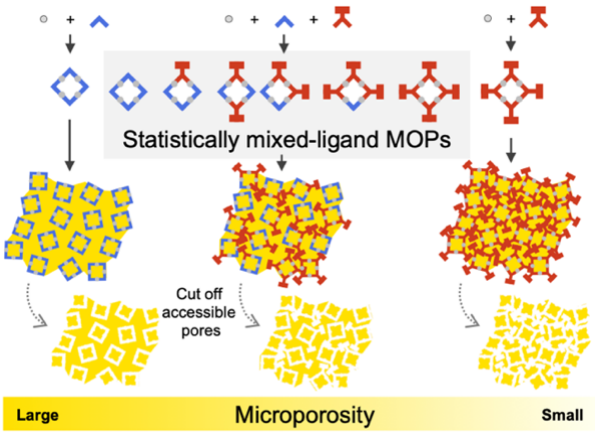

Fig. 1 Schematic illustration of tuning microporosity in amorphous solids of MOPs with different numbers of small (blue) and bulky (red) organic ligands. The yellow area indicates accessible micropores in amorphous solids of MOPs.

HCzRhMOP and **BnCzRhMOP** were synthesized by the reactions of [Rh_2(acetate)$_4$(methanol)$_2$] with either H_2HCz for **HCzRhMOP** or H_2BnCz for **BnCzRhMOP** in *N*,*N*-dimethyl acetamide (DMA) heated at 120°C. The diamagnetic nature of Rh_2 paddlewheels allows us to monitor the reaction of the synthesis of **HCzRhMOP** by ^{1}H NMR spectroscopy and to optimize the reaction time to be 24 h (Fig. S1a). **BnCzRhMOP** was synthesized in 6 h according to the monitoring of the synthetic reaction of **BnCzRhMOP** (Fig. S1b).

HCzRhMOP crystallizes in the monoclinic space group *I*2/*a*. Each Rh_2 dimer unit is coordinated by four HCz ligands to form octahedral geometry (Fig. 2a). The average distance between diagonal Rh_2 paddlewheels in **HCzRhMOP** is estimated to be 19.1 Å for exterior Rh ions and 14.3 Å for interior Rh ions. **HCzRhMOP** has eight window openings of 6.8 Å for triangle apertures, as determined by pywindow software.[25] Four out of six external and two out of six internal axial coordination sites of Rh_2 paddlewheels are coordinated by the crystal solvent DMA. The other sites were modeled as coordinated by oxygen atoms. Here, DMA molecules coordinating the Rh_2 paddlewheels occupy the space around the triangle aperture of neighboring **HCzRhMOP** molecules (Fig. 2c). Such packing mode should be a common feature for this octahedral MOP arrangement because the Cu analog also shows a similar interaction.[21,22] **HCzRhMOP**s are packed in face-centered cubic (fcc) arrangement, in which no π-π stacking interactions between carbazole rings of any neighboring 12 MOPs are found in the crystal structure (Fig. S2).

BnCzRhMOP crystalizes in the trigonal space group *R*–3. **BnCzRhMOP** molecule is geometrically identical to **HCzRhMOP**, except for the benzyl groups attached on the periphery of the MOP (Fig. 2b). Two types of π-π stacking interactions between the neighboring MOPs were observed: one between a benzyl group and a carbazole ring and the other between carbazole rings (Fig. 2d and e). **BnCzRhMOP**s are also packed in fcc, in which 12 carbazole rings and 6 out of 12 benzyl groups contribute to the π-π stacking interactions (Fig. S3).

HCzRhMOP and **BnCzRhMOP** were soluble and stable in coordinative solvents, such as DMA and dimethylsulfoxide (DMSO), which allows us to spectroscopically characterize them in solution. The ^{1}H NMR spectra of **HCzRhMOP** and **BnCzRhMOP** in DMSO-d_6 showed one set of signals from the corresponding ligands (Fig. S1). The UV-Vis absorption spectroscopy for **HCzRhMOP** and **BnCzRhMOP** in DMA showed similar absorption bands (both λ_{max} = 602 nm), corresponding to the π* → σ* electronic transition in a metal–metal bonded Rh_2 paddlewheel (Fig. S5).[26]

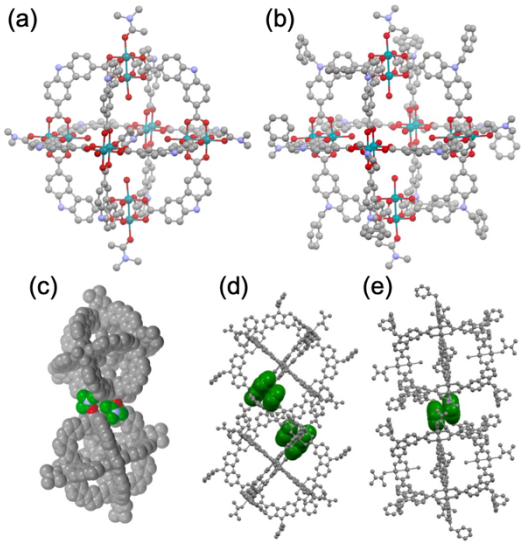

Fig. 2 Crystal structures of (a) **HCzRhMOP** and (b) **BnCzRhMOP**. Crystal solvent molecules and hydrogen atoms were omitted for clarity. (c) Two neighboring **HCzRhMOP**s. DMA molecules are colored in green for carbons, blue for nitrogens, and red for oxygen. (d, e) Two neighboring **BnCzRhMOP**s. π-π stacking interactions between (d) a carbazole ring and a benzyl group and (e) two carbazole rings. Carbazole rings and benzyl groups with space-filling models and colored in green contribute to the π-π stacking interactions between **BnCzRhMOP**s.

We then synthesized mixed-ligand **H/BnCzRhMOPs** from [Rh_2(acetate)$_4$(methanol)$_2$] and both H_2HCz and H_2BnCz in the ratios (H_2HCz/H_2BnCz) of 11/1, 9/3, 6/6, 3/9 or 1/11, respectively, according to the synthetic protocol of **HCzRhMOP**. All solids were obtained as amorphous solids similar to **HCzRhMOP** and **BnCzRhMOP** (Fig. S6a). The diffusion coefficients of all **H/BnCzRhMOPs** in DMSO-d_6 determined by the ^{1}H diffusion ordered spectroscopy (DOSY) experiments are almost identical (ca. 6.0 × 10^{-11} m^2 s^{-1}), corresponding to those of **HCzRhMOP** (5.89 × 10^{-11} m^2 s^{-1}) and **BnCzRhMOP** (6.12 × 10^{-11} m^2 s^{-1}), respectively (Figs. S7–10 and Tables S3–7). These results indicate the sizes of **H/BnCzRhMOPs** are almost same as **HCzRhMOP** and **BnCzRhMOP**. Then, we digested all **H/BnCzRhMOPs** by heating at 100°C in DMSO-d_6/DCl and determined the HCz/BnCz ratio in each MOP by ^{1}H NMR

spectroscopy. The ^{1}H NMR spectra of each digested **H/BnCzRhMOP** indicated that the HCz/BnCz ratio observed corresponds to the precursory ratio of H_2HCz and H_2BnCz used in the syntheses (Figs. 3 and S11).

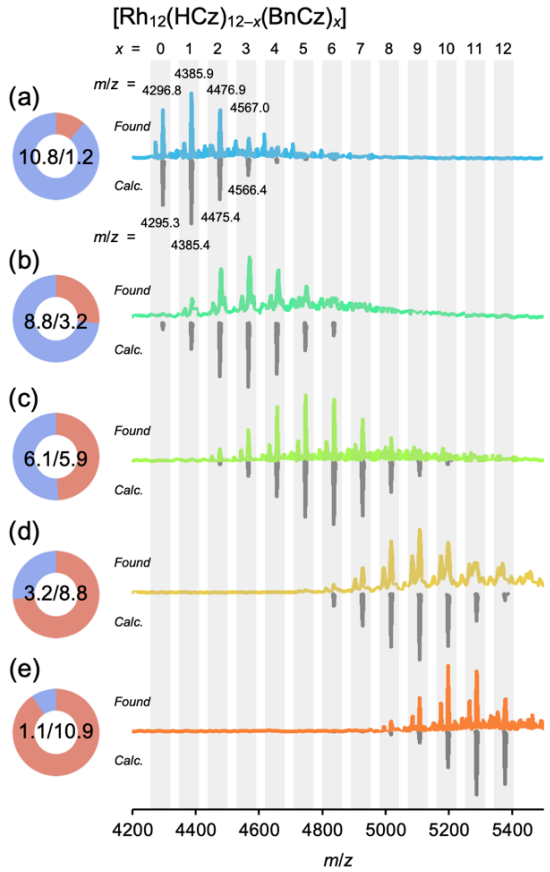

Fig. 3 Compositional ratios of HCz and BnCz determined by ^{1}H NMR spectra shown in the pie charts and MALDI-TOF mass spectra of **H/BnCzRhMOPs**. **H/BnCzRhMOPs** were synthesized from both H_2HCz and H_2BnCz in the ratios (H_2HCz/H_2BnCz) of (a) 11/1 (light blue), (b) 9/3 (green), (c) 6/1 (light green), (d) 3/9 (yellow) and (e) 1/11 (orange), respectively. Spectra colored in gray correspond to the calculated signal pattern.

The MALDI-TOF mass measurements supported those compositional ratios (Fig. 3). For instance, a **H/BnCzRhMOP** sample synthesized from the 11/1 ratio of H_2HCz and H_2BnCz shows the most intense signal at *m/z* 4385.9, corresponding to the mixed-ligand MOP $[Rh_{12}(HCz)_{11}(BnCz)_1 + Na]^+$ (calc. *m/z* 4385.4) (Figs. 3a and S12a). Besides this major signal, there are several MOP signals of $[Rh_{12}(HCz)_{12-x}(BnCz)_x + Na]^+$ with *x* values different from the precursory ratio (x = 1) of HCz and BnCz ligands, x = 0 (*m/z* found 4296.8, calc. 4295.3), 2 (*m/z* found 4476.9, calc. 4475.4), and 3 (*m/z* found 4567.0, calc. 4566.4). The signals matched with the calculated signal pattern where both HCz and BnCz ligands are statistically distributed within each MOP according to the average compositional ratio determined by ^{1}H NMR spectroscopy as discussed above. Similar distributions are found in the other **H/BnCzRhMOP** samples (Figs. 3 and S12). Therefore, we obtained and spectroscopically characterized five types of mixed-ligand **H/BnCzRhMOPs** (HCz/BnCz = 11/1, 9/3, 6/6, 3/9 and 1/11, respectively).

With **HCzRhMOP**, **BnCzRhMOP** and five types of **H/BnCzRhMOPs**, we investigated the structure–porosity relationship of the MOPs containing different numbers of the benzyl groups. To compare the gas sorption properties, the thermal stabilities of the MOPs were investigated. Thermogravimetric analyses showed the decomposition temperatures of all the MOPs to be almost equal around 300°C (Fig. S13). PXRD experiments confirmed that all the samples were amorphous after the activation at 120°C in vacuo (Fig. S6b). IR spectroscopy experiments showed no significant difference before and after the activation. This result confirms the structural integrity of all the MOPs after the activation, thanks to the strong coordination bonds between Rh_2 core and the equatorial carboxylates (Fig. S14).

To reveal the structure–porosity relationship, we first compared the N_2 sorption isotherms of **HCzRhMOP** and **BnCzRhMOP** measured at 77 K (Figs. 4a and S15). Both **HCzRhMOP** and **BnCzRhMOP** show type I sorption isotherms, which indicates that both MOP amorphous solids have microporosity.[13] The total uptake at $P/P_0 \approx 1$ in **HCzRhMOP** (283 cm^3(STP) g^{-1}) is higher than that in **BnCzRhMOP** (121 cm^3(STP) g^{-1}). The Brunauer–Emmett–Teller (BET) surface areas of **HCzRhMOP** and **BnCzRhMOP** are calculated to be 877 and 319 m^2 g^{-1} by BETSI[27] (Table S8).

To understand the effect of the benzyl groups on microporosity in more detail, we analyzed the adsorption data using the Dubinin-Radushkevich equation.[28] This analysis calculates the adsorbed volume of adsorbent in the microporosity of the samples (Fig. S16). The micropore volume in the amorphous solids of **HCzRhMOP** is 224 cm^3 g^{-1}, accounting for 79% of the total adsorbed volume of N_2. In the same way, the amorphous solids of **BnCzRhMOP** have a micropore volume of 85 cm^3 g^{-1}, which corresponds to 70% of the total adsorbed volume of N_2. These results indicate that a large part of the porosity in these amorphous solids stems from the microporosity and the relative contribution from the microporosity is nearly equal in these two MOP samples. The decrease in microporosity with the benzyl groups was also confirmed when considering the difference in the molecular weights. The number of adsorbed N_2 molecules at $P/P_0 \approx 0.1$ per **BnCzRhMOP** (19.5 mol(N_2) mol^{-1}(MOP)) was almost half (45%) of that per **HCzRhMOP** (43.3 mol(N_2) mol^{-1}(MOP)). To clarify the bulkiness of benzyl groups, the void volume in the unit cell of each crystal structure of **HCzRhMOP** and **BnCzRhMOP** without any coordinating solvent molecules was estimated to be 28.1% and 12.4%, respectively. This difference in the void volume of **BnCzRhMOP**/**HCzRhMOP** is calculated to be 44%, which is consistent with the difference in adsorbed amounts of 45% (Fig. S4 and Table S8).

This analysis indicates that the density of molecules in the crystalline phase is reflected in the corresponding amorphous phase after the activation. Indeed, the adsorption isotherms of the amorphous solids of the mixed-ligand **H/BnCzRhMOPs** can be plotted between those of two homoleptic MOPs (Figs. 4a and S15b–f). The microporosity in each MOP sample linearly decreases, depending on the number of the benzyl groups (Fig. 4b and Table S8). The physical mixture of **HCzRhMOP** and **BnCzRhMOP** (6/6) shows a similar sorption isotherm to **H/BnCzRhMOP** (HCz/BnCz = 6/6; Figs. S15d and h). These

similar sorption properties indicate that in the mixed-ligand MOPs there is no specific molecular arrangement that affects the microporosity. In addition, the CO_2 adsorption isotherms of all MOP samples were measured at 195 K and showed the same trend observed in the N_2 adsorption experiments (Figs. S17 and S18 and Table S9). Therefore, this systematic study reveals that the porosity of the amorphous solids of MOPs can be evaluated based on the structure-porosity relationship derived from the corresponding crystal structures of MOPs.

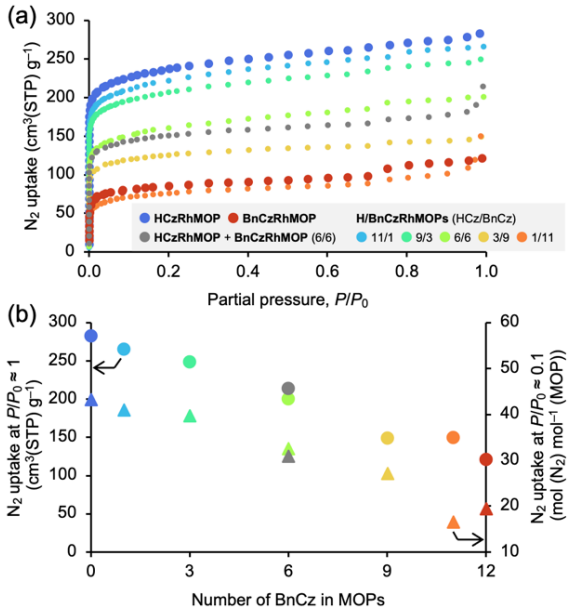

Fig. 4 (a) N_2 adsorption isotherms of all **HCzRhMOP**, **BnCzRhMOP** and **H/BnCzRhMOPs** measured at 77 K. For clarity, only the adsorption branches are shown, and desorption data are given in the SI. (b) The adsorbed N_2 gas for MOP samples against the number of BnCz in MOPs at $P/P_0 \approx 1.0$ with a volumetric and gravimetric scale (circle symbols and the left y-axis) and at $P/P_0 \approx 0.1$ with a molar scale (triangle symbols and the right y-axis).

In conclusion, we demonstrated an approach to tuning the microporosity in the amorphous solids of systematically synthesized **HCzRhMOP**, **BnCzRhMOP** and mixed-ligand **H/BnCzRhMOPs**. **H/BnCzRhMOPs** have the statistical distribution of the HCz and BnCz ligands, and the number of the benzyl groups linearly correlates with the decrease in the microporosity because the void is partially occupied by the benzyl groups. This study unveils that the porosity in MOP-based amorphous solids can be correlated to the crystal structures of the corresponding ordered MOP assemblies. This research will be helpful for further research with MOPs and other molecular porous materials to design the porosities.

T. T. and J. T. are grateful to the Japan Society for the Promotion of Science (JSPS) for the postdoctoral fellowship. This work was supported by JSPS KAKENHI grant number 22KJ1784 (JSPS Fellows) and 23K13762 (Early-Career Scientists) for T. T. and 23H00298 (Kiban A) for S. F. The authors thank the iCeMS Analysis Centre for access to analytical instruments and Ms. Karin Nishimura (Kyoto University) for assistance in the mass spectrometry measurements.

Conflicts of interest

There are no conflicts to declare.

Notes and references

1. M. Eddaoudi, J. Kim, J. B. Wachter, H. K. Chae, M. O'Keeffe and O. M. Yaghi, *J. Am. Chem. Soc.*, 2001, **123**, 4368–4369.
2. T. Tateishi, M. Yoshimura, S. Tokuda, F. Matsuda, D. Fujita and S. Furukawa, *Coord. Chem. Rev.*, 2022, **467**, 214612.
3. A. C. Sudik, A. R. Millward, N. W. Ockwig, A. P. Cote, J. Kim and O. M. Yaghi, *J. Am. Chem. Soc.*, 2005, **127**, 7110–7118.
4. Y. Gu, E. A. Alt, H. Wang, X. Li, A. P. Willard and J. A. Johnson, *Nature*, 2018, **560**, 65–69.
5. X. Y. Xie, F. Wu, X. Liu, W. Q. Tao, Y. Jiang, X. Q. Liu and L. B. Sun, *Chem. Commun.*, 2019, **55**, 6177–6180.
6. E. V. Perez, K. J. Balkus, J. P. Ferraris and I. H. Musselman, *J. Membr. Sci.*, 2014, **463**, 82–93.
7. E. Sanchez-Gonzalez, M. Y. Tsang, J. Troyano, G. A. Craig and S. Furukawa, *Chem. Soc. Rev.*, 2022, **51**, 4876–4889.
8. A. J. Gosselin, C. A. Rowland and E. D. Bloch, *Chem. Rev.*, 2020, **120**, 8987–9014.
9. S. Kitagawa, R. Kitaura and S. Noro, *Angew. Chem. Int. Ed.*, 2004, **43**, 2334–2375.
10. B. Lee, I. H. Park and J. Park, *ACS Materials Lett.*, 2022, **4**, 2388–2393.
11. B. Lee, B. Go, B. Jung and J. Park, *Small*, 2023, DOI: 10.1002/smll.202308393.
12. M. M. Deegan, A. M. Antonio, G. A. Taggart and E. D. Bloch, *Coord. Chem. Rev.*, 2021, **430**, 213679.
13. S. Furukawa, N. Horike, M. Kondo, Y. Hijikata, A. Carne-Sanchez, P. Larpent, N. Louvain, S. Diring, H. Sato, R. Matsuda, R. Kawano and S. Kitagawa, *Inorg. Chem.*, 2016, **55**, 10843–10846.
14. J. Albalad, L. Hernandez-Lopez, A. Carne-Sanchez and D. Maspoch, *Chem. Commun.*, 2022, **58**, 2443–2454.
15. G. R. Lorzing, A. J. Gosselin, B. A. Trump, A. H. P. York, A. Sturluson, C. A. Rowland, G. P. A. Yap, C. M. Brown, C. M. Simon and E. D. Bloch, *J. Am. Chem. Soc.*, 2019, **141**, 12128–12138.
16. G. A. Taggart, A. M. Antonio, G. R. Lorzing, G. P. A. Yap and E. D. Bloch, *ACS Appl. Mater. Interfaces*, 2020, **12**, 24913–24919.
17. A. M. Antonio, K. J. Korman, G. P. A. Yap and E. D. Bloch, *Chem. Sci.*, 2020, **11**, 12540–12546.
18. B. Lerma-Berlanga, J. Castells-Gil, C. R. Ganivet, N. Almora-Barrios, J. Gonzalez-Platas, O. Fabelo, N. M. Padial and C. Marti-Gastaldo, *J. Am. Chem. Soc.*, 2021, **143**, 21195-21199.
19. A. M. Antonio, K. J. Korman, M. M. Deegan, G. A. Taggart, G. P. A. Yap and E. D. Bloch, *Inorg. Chem.*, 2022, **61**, 4609–4617.
20. B. Doñagueda Suso, Z. Wang, A. Kennedy, A. J. Fletcher, S. Furukawa and G. Craig, *Chem. Sci.*, 2024, DOI: 10.1039/d3sc06140j.
21. J. R. Li, D. J. Timmons and H. C. Zhou, *J. Am. Chem. Soc.*, 2009, **131**, 6368–6369.
22. A. López-Olvera, E. Sánchez-González, A. Campos-Reales-Pineda, A. Aguilar-Granda, I. A. Ibarra and B. Rodríguez-Molina, *Inorg. Chem. Front.*, 2017, **4**, 56–64.
23. C. A. Rowland, G. P. A. Yap and E. D. Bloch, *Dalton Trans.*, 2020, **49**, 16340–16347.
24. L. J. Weselinski, R. Luebke and M. Eddaoudi, *Synthesis*, 2014, **46**, 596–599.
25. M. Miklitz and K. E. Jelfs, *J. Chem. Inf. Model.*, 2018, **58**, 2387–2391.
26. E. B. Boyar and S. D. Robinson, *Coord. Chem. Rev.*, 1983, **50**, 109–208.
27. J. W. M. Osterrieth, et al., *Adv. Mater.*, 2022, **34**, e2201502.
28. M. M. Dubinin and L. V. Radushkevich, *Proc. Acad. Sci. USSR*, 1947, **55**, 331–333.